Research Article

MOLECULAR PAIN

Molecular Pain
Volume 21: 1–16

DOI: 10.1177/17448069251324645
journals.sagepub.com/home/mpx
Sage

Upregulation of LRRC8A in the anterior cingulate cortex mediates chronic visceral pain in adult male mice with neonatal maternal deprivation

Jin-Nan Lu[1], Jing-Heng Dou[2], Zi-Long Yi[1], Lian Lian[3], Xing-Lei Ben[4], Fu-Chao Zhang[2,3], and Guang-Yin Xu[1,2]

Abstract

Irritable bowel syndrome (IBS) is a functional gastrointestinal disorder primarily characterized by chronic visceral pain. Studies have reported that the anterior cingulate cortex (ACC) is involved in chronic visceral pain, however, the molecular mechanisms underlying this involvement remain largely unclear. In this study, we aimed to investigate the molecular mechanisms of the ACC in chronic visceral pain induced by neonatal maternal deprivation (NMD) in male mice. We showed that the expression of leucine-rich repeat-containing protein family member 8A (LRRC8A) at both mRNA and protein levels was significantly upregulated in the ACC of NMD male mice, with LRRC8A primarily co-localized in neurons. DCPIB, an inhibitor of LRRC8A, greatly alleviated chronic visceral pain. Moreover, the ATP concentration was significantly upregulated in the ACC of NMD male mice. However, LRRC8A was not involved in somatic pain induced by complete Freund's adjuvant (CFA) injection into the hind paw. In conclusion, our findings demonstrate that LRRC8A plays a critical role in regulating chronic visceral pain in NMD mice. These findings are expected to provide new ideas for the treatment of chronic visceral pain in IBS patients.

Keywords

Irritable bowel syndrome, chronic visceral pain, LRRC8A, anterior cingulate cortex, ATP

Date received: 8 December 2024; revised 11 February 2025; accepted: 12 February 2025

Introduction

Chronic pain is mainly caused by nerve damage, tissue inflammation, and tumor invasion,[1] representing a significant health issue. Chronic visceral pain, in particular, is a long-lasting and poorly localized pain caused by disorders of the internal organs.[2] Its prevalence exceeds 20% of the global population[3] and is a common symptom in patients with gastrointestinal disorders and various other diseases.[4] Irritable bowels syndrome (IBS) is a functional gastrointestinal disorder primarily characterized by chronic visceral pain and altered intestinal motility.[5–8] Research indicates that the global prevalence of IBS ranges from 1.1% to 45%,[9] severely impacting patients' quality of life and imposing a significant economic and social burden. IBS is often associated with psychological abnormalities such as anxiety, stress, and

[1]Henan Key Laboratory of Child Brain Injury and Henan Pediatric Clinical Research Center, The Third Affiliated Hospital and Institute of Neuroscience of Zhengzhou University, Zhengzhou, Henan, P. R. China
[2]Jiangsu Key Laboratory of Neuropsychiatric Diseases and Institute of Neuroscience, Soochow University, Suzhou, Jiangsu, P. R. China
[3]Department of Oncology, Suzhou Xiangcheng People's Hospital, Suzhou, Jiangsu, P. R. China
[4]Department of Orthopedics, Clinical Medicine Institute of Soochow University and Suzhou BenQ Medical Center, Suzhou, Jiangsu, P. R. China

Corresponding Authors:
Guang-Yin Xu, Laboratory of Translational Pain Medicine, Institute of Neuroscience, Soochow University, 199 Renai Road, Suzhou, Jiangsu 215123, P.R. China.
Email: guangyinxu@suda.edu.cn

Fu-Chao Zhang, Laboratory of Translational Pain Medicine, Institute of Neuroscience, Soochow University, 199 Renai Road, Suzhou, Jiangsu 215123, P.R. China.
Email: fczhang@suda.edu.cn

depression.[10,11] However, the pathophysiological mechanism of IBS remains incompletely understood. It is currently thought to be a combination of multiple factors leading to abnormal gut-brain interaction abnormalities.[11–13] Additionally, the literature suggests that early life stress is a high-risk factor for the development of chronic visceral pain in adulthood.[14,15] Visceral hypersensitivity is a common clinical manifestation of IBS.[16,17] To simulate the clinical manifestations observed in IBS patients, chronic visceral pain can be induced in offspring adult mice through the neonatal maternal deprivation (NMD) model, and visceral hypersensitivity can be assessed using colorectal distention (CRD).[18,19]

The anterior cingulate cortex (ACC) is situated in the anterolateral part of the cerebral cortex, contains several regions and a variety of molecules crucial for pain modulation and pain-related mood disorders.[20–29] Substantial evidence indicates that the ACC is involved in modulating various types of chronic pain, including neuropathic pain and inflammatory pain.[30–35] Recently, our group demonstrated that ACC-related circuits were involved in mediating chronic visceral pain,[2] but the underlying molecular mechanisms are not yet well understood.

The volume-regulated anion channel (VRAC) consists of leucine-rich repeat-containing protein family member 8A (LRRC8A) subunits.[36] DCPIB, a potent inhibitor of VRAC,[37–40] is capable of binding to the VRACs like a "barrel bung" to exert its inhibitory effect.[41,42] Previous studies have shown that LRRC8A is involved in the regulation of neuropathic pain,[43] and there is also evidence that LRRC8A plays a crucial role in the mechanisms that mediate ATP release.[44] It can mediate an increase in ATP release to promote the development of chronic neuropathic pain.[45] However, the role of LRRC8A in chronic visceral pain remains unclear. Studies have shown that ATP-mediated purinergic signaling plays an important regulatory role in chronic pain.[46–48] In addition, some research demonstrated that ATP-mediated purinergic signaling is involved in the regulation of chronic visceral pain in the mouse spinal cord and other brain disorders.[49,50]

Therefore, we hypothesize that the VRAC channel composed of LRRC8A may be involved in regulating chronic visceral pain through ATP release. In the present study, we demonstrated that LRRC8A, predominantly expressed in the neurons of the ACC in NMD male mice, were involved in regulating chronic visceral pain through ATP release. This finding is anticipated to offer new insights into the treatment of chronic visceral pain in patients with IBS.

Materials and methods

Animals

SPF-grade wild-type C57BL/6J mice, weighing 22–25 g and aged 6 weeks and above, were purchased from Beijing Vital River Laboratory Animal Technology Co., Ltd. and housed in the Laboratory Animal Breeding Center of the Department of Clinical Research and Translational Medicine of the Third Affiliated Hospital of Zhengzhou University. Female and male mice were used for breeding, modeling, and experiments. All mice were housed in a standardized environment with the stocking density controlled at 1–5 mice per cage, temperature maintained at 20–25°C, relative humidity at 40%–70%, and treated with a 12/12-h light/dark cycle. All mice were provided with adequate space and free access to water and food. All animal experiments were performed in strict compliance with the guidelines of the International Association for the Study of Pain and were approved by the Ethics Committee of the Third Affiliated Hospital of Zhengzhou University.

Induction of chronic visceral pain

Referring to the previous modeling methods of our group,[18] we induced chronic visceral pain in mice by establishing a model of neonatal maternal deprivation (NMD). NMD group: The offspring mice were given 3 h of isolation stress at a fixed time every day from day 2 to day 15 after birth. Mice were carefully removed from their mother each day and placed in a custom-made molding box, which consisted of multiple compartments of equal proportions, each mouse was placed in a separate compartment. At the end of two consecutive weeks of mother-infant separation, the mice were kept normally with their mother. CON group: The offspring mice were born without any treatment and fed normally with their mother. Both groups of mice were kept in separate cages from their mother on the 21st day after birth, and behavioral and subsequent experiments were conducted after the mice reached 42 days of age.

Induction of somatic pain

The modeling subjects were 6-week-old healthy offspring adult male mice with somatic pain induced by the use of complete Freund's adjuvant (CFA).[51,52] CFA group: The mice were anesthetized with isoflurane, and 25 μL of CFA (MedChemExpress, USA) was injected into the left hind paw of the mice, followed by returning the mice to their cages for normal rearing. Normal saline (NS) group: Mice were injected with 25 μL of 0.9% saline into the left hind paw, and all other procedures were the same as those for CFA mice. Compared with NS mice, the left hind paw of CFA mice showed significant swelling on days 1–3 after modeling, and the experiments were performed 3 days after modeling.

Measurement of chronic visceral pain

In this experiment, visceral pain thresholds in mice were detected by colorectal distension (CRD),[18] specific operations are as follows. The mouse was deeply anesthetized with

Table 1. Primer sequences used for qPCR.

Gene	Primers	Sequences (5'-3')
GAPDH	Forward	AACTTTGGCATTGTGGAAGG
GAPDH	Reverse	GGATGCAGGGATGATGTTC
LRRC8A	Forward	AGCTCTTCTACTGCCGCAAG
LRRC8A	Reverse	GGGGAGCGCTTCAATCCTATT
P2X1R	Forward	TCCTGCCTAAGAGGCACTACT
P2X1R	Reverse	GTCACGTTCACCCTCCCCAG
P2X2R	Forward	GTTCTGGGACTACGAGACGC
P2X2R	Reverse	CGATGAAGACGTACCACACGA
P2X3R	Forward	CTCCTACTTTGTGGGGTGGG
P2X3R	Reverse	ACTCTGTTGGCATAGCGTCC
P2X4R	Forward	GCGTCTGTGAAGACCTGTGA
P2X4R	Reverse	AAAAAGCTGGCGTTGGCAC
P2X5R	Forward	TCGAGCCTGCCAGAGAAAAG
P2X5R	Reverse	CACAGAGGCAGAGAGAAGGC
P2X6R	Forward	TGCTGTGCCCAGATCCAATG
P2X6R	Reverse	AGTACGGACTGGAGAGTGGA
P2X7R	Forward	AGGCCAAGAAGTTCCAACCTA
P2X7R	Reverse	TCCATTGAGAGCATGGCTTCTT
P2Y1R	Forward	TCAAGCAGAATGGAGACACGA
P2Y1R	Reverse	GCAGGTTCAAAGCAACCATGT
P2Y2R	Forward	GCAGCGGGGAGGAGTC
P2Y2R	Reverse	GGACTGAGGCAGGAAACAGG
P2Y4R	Forward	CACCGGGTAGGAGTCTTGTC
P2Y4R	Reverse	GGGTAAGGAGCACCATCTTAGT
P2Y6R	Forward	CAGAGGGAGTTTTCAGATAAACGG
P2Y6R	Reverse	CAGAGAGCTCTGGTGGCTTTT
P2Y12R	Forward	AGGGTCACAGTGCAAGAACAC
P2Y12R	Reverse	TGGAACTTGCAGACTGGCAT
P2Y13R	Forward	TGGGTTGAGCTAGTAACTGCC
P2Y13R	Reverse	TTGTCCCGAGCATCAGCTTT
P2Y14R	Forward	TACGGATGGGGACGGGG
P2Y14R	Reverse	ACCTCTGGAGGCAAAGATTTTCT

isoflurane. The head of the mouse was placed in an air anesthesia mask so that the mouse would not wake up during the operation. Then, a medical cotton swab was dipped in Vaseline and applied fully and evenly to the unexpanded homemade balloon and the mouse's anus. The catheter is a PE90 catheter with a length of about 10 cm, and a latex balloon with a length of about 1.5 cm is connected to the end of the catheter. The connection between the two is wrapped and tied with sutures, and the part wrapped with sutures is sealed with sealing film. Then the balloon coated with Vaseline was slowly inserted from the mouse's anus to a depth of 2 cm into the colorectum. Finally, the catheter of the balloon was fixed to the root of the mouse tail with pressure-sensitive tape, and the mouse was transferred to a dedicated horizontal table. After the mouse was awake and adapted for 30 min, behavioral testing was performed. The three-way tube was connected to the external catheter of the sphygmomanometer, syringe, and airbag respectively. After the mouse was adapted, the balloon was slowly ventilated, and the reading of the sphygmomanometer rose until the mice exhibited visceral pain behaviors such as abdominal contractions or head raising. At this point, the gas injection was stopped, and the sphygmomanometer reading was recorded. Each mouse was counted five times, with a 5-min interval between each measurement. The average of the five counts was taken as the visceral pain threshold of the mouse. Each mouse was tested in the same way.

Measurement of somatic pain

Before the experiment, the NS and CFA groups of mice were placed on a wire mesh rack (RWD, China) to adapt to the environment, and then behavioral tests were performed to evaluate the pain thresholds of the mice. The specific operations were as follows: 3 days before the start of the experiment, the two groups of mice to be tested were fixed and placed on a wire mesh rack for 30 min every day using a transparent resin box (RWD, China) to adapt to the environment. On the day of the experiment, after the mice were fixed on the mesh rack, they were also allowed to stand for 30 min to adapt to the environment. After that, a 0.008–2.0 g Von Frey needle was used to stimulate the sole of the left foot of the mouse,[53] and the paw withdrawal threshold (PWT) of the left foot of the mouse was measured as the threshold of the somatic pain.[54,55]

Real-time quantitative PCR (qPCR)

qPCR technology was used to quantitatively determine the mRNA expression of related genes. The brain tissue samples obtained the day before were taken out of the −80°C refrigerator and placed in an ice box. The total RNA of the specific brain tissue was extracted using RNAsimple Total RNA Kit (TIANGEN, China) according to its instructions. Then, the RNA concentration was measured using a nanodrop instrument, and the total RNA with the measured concentration was reverse transcribed into cDNA according to the reverse transcription kit Hifair® III 1st Strand cDNA Synthesis SuperMix for qPCR (gDNA digester plus). Then, the qPCR system was configured according to the instructions of the kit Hieff® qPCR SYBR Green Master Mix (NoRox) and the LightCycler 96 (Roche, Switzerland) instrument was used for real-time fluorescence quantitative PCR. The primer sequences used for qPCR are shown in Table 1. Finally, the ΔΔCt method was used for data analysis.

Western blotting

The mice were anesthetized using the anesthetic Zoletil 100 (Virbac, France), followed by cardiac perfusion with 0.9% saline and removal of brain tissues from the ACC, HIP, PFC, and IC, which were rapidly placed in liquid nitrogen. Then, the extraction of total protein was performed, and the operation process was carried out on ice. We first added

Table 2. Antibodies used for WB.

Type	Antibodies	Dilution
Primary antibodies	Anti-GAPDH (Cell Signaling Technology, USA)	1:1000
	Anti-LRRC8A (Santa Cruz Biotechnology, USA)	1:1000
	Anti-P2X4R (Proteintech, China)	1:1000
	Anti-P2Y12R (Abcam, UK)	1:1000
Secondary antibodies	Goat anti-rabbit IgG H&L HRP (Abcam, UK)	1:10000
	Goat anti-mouse IgG H&L HRP (Thermo Fisher Scientific, USA)	1:10000

Table 3. Primary antibodies are used for immunofluorescence staining.

Antibodies	Dilution
Anti-LRRC8A (Alomone Labs, Israel)	1:200
Anti-NeuN (Oasis Biofarm, China)	1:400
Anti-Iba1 (Oasis Biofarm, China)	1:400
Anti-GFAP (Cell Signaling Technology, USA)	1:600

RIPA lysate (YEASEN, China), phosphatase inhibitor (Selleck, USA), and protease inhibitor (Selleck, USA) sequentially in the ratio of 100:2:1 to form a sample lysate mixture, and then 206 μL of the lysate mixture was added to each sample, ultrasonically fragmented, and reacted on ice for 10 min. Afterward, the samples were centrifuged at 4°C for 30 min at 12,000 rpm. After centrifugation, the supernatant was aspirated in a new 1.5 mL centrifuge tube and the total protein concentration was determined by using the BCA Protein Concentration Measurement Kit (Beyotime, China). The protein system was prepared according to the measured protein concentration and heated in a metal bath at 95°C for 10 min to denature the protein. Extracted protein samples were electrophoresed using a 15-well 4%–20% high-resolution precast gel (YEASEN, China) at a constant voltage of 100 V for 70 min, followed by transferring the proteins onto PVDF membranes (Millipore, USA) at a constant current of 300 mA for 60 min. The PVDF membranes were sealed with 6% skimmed milk closed at room temperature for 2 h, after which the membranes were transferred to a solution containing primary antibody and incubated at 4°C overnight. The next morning, the membranes were transferred to the solution containing the secondary antibody and incubated at room temperature for 2 h. The primary and secondary antibodies used in this experiment are shown in Table 2. Finally, the proteins on the membranes were observed using the ECL Ultrasensitive Chemiluminescence Detection Kit (Epizyme, China) and analyzed using ImageLab.

Immunofluorescence staining

Mice were anesthetized using the anesthetic Zoletil 100 and then perfused sequentially with 0.9% saline and 4% paraformaldehyde (Biosharp, China) in the heart, and the whole brain of the mice were removed and immediately placed in 4% paraformaldehyde for fixation for 24 h. After fixation, the samples were dehydrated by gradient ethanol in a dehydrator (DIAPATH, Milan), and were transparent in xylene. Next, paraffin (CITOTEST, China) embedding was performed at 52–54°C using an embedding machine (WHJJ, China). After that, conventional sectioning was performed using a pathology slicer (Leica Biosystems, China), and mouse brains were sliced to 4–10 μm thickness and pasted onto treated clean slides (CITOTEST, China). After that, the slices were baked at 34°C overnight collected in a mounting box and stored at 4°C in a sealed box. We used the Multiplex Immunofluorescence Staining Kit (DINGHANBIOTECH, China) for immunofluorescence staining, and we referred to the instruction manual of the kit for details, and the general procedure was as follows. First, the sections were put into dewaxing solution and different concentrations of anhydrous ethanol for dewaxing and dehydration in turn, followed by antigen repair with EDTA antigen repair solution in a microwave oven, and then cooled naturally and washed the slides in PBS (pH = 7.4) for three times, each time for 5 min. Next, the sections were blocked from endogenous peroxidase by placing them in 3% hydrogen peroxide solution, incubated at room temperature and protected from light for 15 min, and then blocked with 10% goat serum at room temperature for 30 min. Subsequently, the sections titrated with primary antibody were incubated at 4°C overnight. On the next day, the brain slices were washed with PBS and incubated with secondary antibody for 50 min at room temperature, followed by the addition of TSA fluorescent dye reaction solution to the slices for 15 min at room temperature, washing of the brain slices with PBS for three times, and elution of the antibody with the antigen repair solution at 95°C for 25 min to complete the one-step fluorescent labeling. Repeat the steps after antigen repair to complete the twofold fluorescence labeling. Finally, the nuclei were restrained with DAPI, sealed, and photographed by microscopic examination, and the number of cells was counted. The primary antibody used in this experiment is shown in Table 3, and the secondary antibody is the HRP goat anti-rabbit/mouse universal secondary antibody that comes with the kit. Immunofluorescence images for display were captured using a laser confocal microscope (LSM900, ZEISS, Germany), and cell counting was performed using ImageJ software.

Stereotaxic injection

The mice were anesthetized with the anesthetic Zoletil 100 and fixed on a brain stereotaxic instrument (RWD, China). According to the mouse brain atlas, the drug administration cannula (RWD, China) was buried in the right ACC (AP: +1.0 mm, ML: +0.4 mm, DV: −1.75 mm) of the mouse. Each mouse was then placed in a cage. After the mice recovered for 3 days, 1 μL DMSO (Glpbio, USA) and 1 μL DCPIB (MedChemExpress, USA) were injected into the ACC of the mice respectively, and the CRD thresholds before and after drug administration were detected. In this experiment, several different drug administration concentrations were set by consulting the literature,[56] and then the optimal drug administration concentration was determined by a single brain stereotaxic administration. Finally, the drug was administered for seven consecutive days to evaluate the drug efficacy time.

ATP test

The Enhanced ATP Assay Kit (Beyotime, China) was used to detect the ATP concentration in the ACC.[57–59] The specific operation process was carried out according to the manufacturer's instructions. Specific methods are briefly described below. The ACC brain tissues were taken first, then added 100 μL of lysis solution to each sample and homogenized it. After centrifugation (4°C, 12,000 g, 5 min) and took the supernatant, which was the tissue sample to be tested. Subsequently, we used ATP standard solution and ATP detection lysis solution to prepare several standard solutions of different concentrations. ATP detection reagent and ATP detection reagent diluent were prepared into ATP detection working solution at a ratio of 1:4. After that, we first added 100 μL of ATP detection working solution to the 96-well plate and placed it at room temperature for 5 min. Then, 60 μL of the sample to be tested or the prepared standard solution was added to each well, and the luminescence of each well was detected by a multifunctional microplate reader (TECAN, Switzerland), and a standard curve was drawn to calculate the ATP concentration of each sample.

Statistical analysis

All data in this study were expressed as Mean ± SEM and were statistically analyzed and graphed using GraphPad Prism 9.5.0 (GraphPad Software, USA). All comparisons between two groups in this study were made using a t-test (Student's *t*-test), and comparisons between multiple groups were made using two-way repeated measure ANOVA (Sidak's multiple comparisons test). Data were considered statistically significant when $p < 0.05$.

Results

NMD induced chronic visceral pain in male mice

To assess chronic visceral pain in mice, the NMD model was established. The timeline of pain threshold detection was shown in Figure 1(a). Visceral pain thresholds were detected by CRD, and it was found that CRD thresholds were significantly downregulated in all NMD male mice at 6–12 weeks compared to CON male mice, indicating that NMD male mice exhibited chronic visceral pain at 6–12 weeks (Figure 1(b), $n = 6$, $^{***}p < 0.001$, two-way ANOVA). To verify whether NMD could induce chronic visceral pain in female mice, CRD tests were performed on 6-week-old CON and NMD female mice, and it was found that there was no significant difference in CRD thresholds between the two groups, indicating that NMD could not induce chronic visceral pain in female mice (Figure 1(c), $n = 6$, Student's *t*-test). Next, to verify whether NMD could induce somatic pain in mice, the paw withdrawal thresholds (PWT) were detected by Von Frey mechanical stimulation. There was no significant difference in the PWT of both CON and NMD male mice at 6–12 weeks, indicating that NMD could not induce somatic pain in male mice (Figure 1(d), $n = 6$, two-way ANOVA). In addition, there was no significant difference in PWT between CON and NMD female mice at 6 weeks of age, indicating that NMD could not induce somatic pain in female mice (Figure 1(e), $n = 8$, Student's *t*-test). These results suggest that NMD induced persistent chronic visceral pain, but not somatic pain in male mice.

LRRC8A expression in the ACC was significantly elevated in NMD male mice

To investigate the molecular mechanisms underlying chronic visceral pain in NMD mice, qPCR and western blotting were employed to assess changes in the expression of mRNA and protein levels in the ACC of CON and NMD mice, respectively. The relative mRNA expression of LRRC8A was significantly upregulated in NMD male mice compared to CON male mice (Figure 2(a), $n = 4$, $^{**}p < 0.01$, Student's *t*-test). The western blotting results revealed that the protein expression of LRRC8A was significantly upregulated in the ACC of NMD male mice compared to CON male mice (Figure 2(b), $n = 6$, $^{**}p < 0.01$, Student's *t*-test). To explore the expression of LRRC8A in several other pain-related brain regions, a western blotting assay was performed. There were no significant differences in the protein levels of LRRC8A between both groups of mice in the hippocampus (HIP), prefrontal cortex (PFC), and insular cortex (IC; Figure 2(c–e), $n = 6$, Student's *t*-test). This suggests that the upregulation of LRRC8A expression in NMD male mice is brain-region specific.

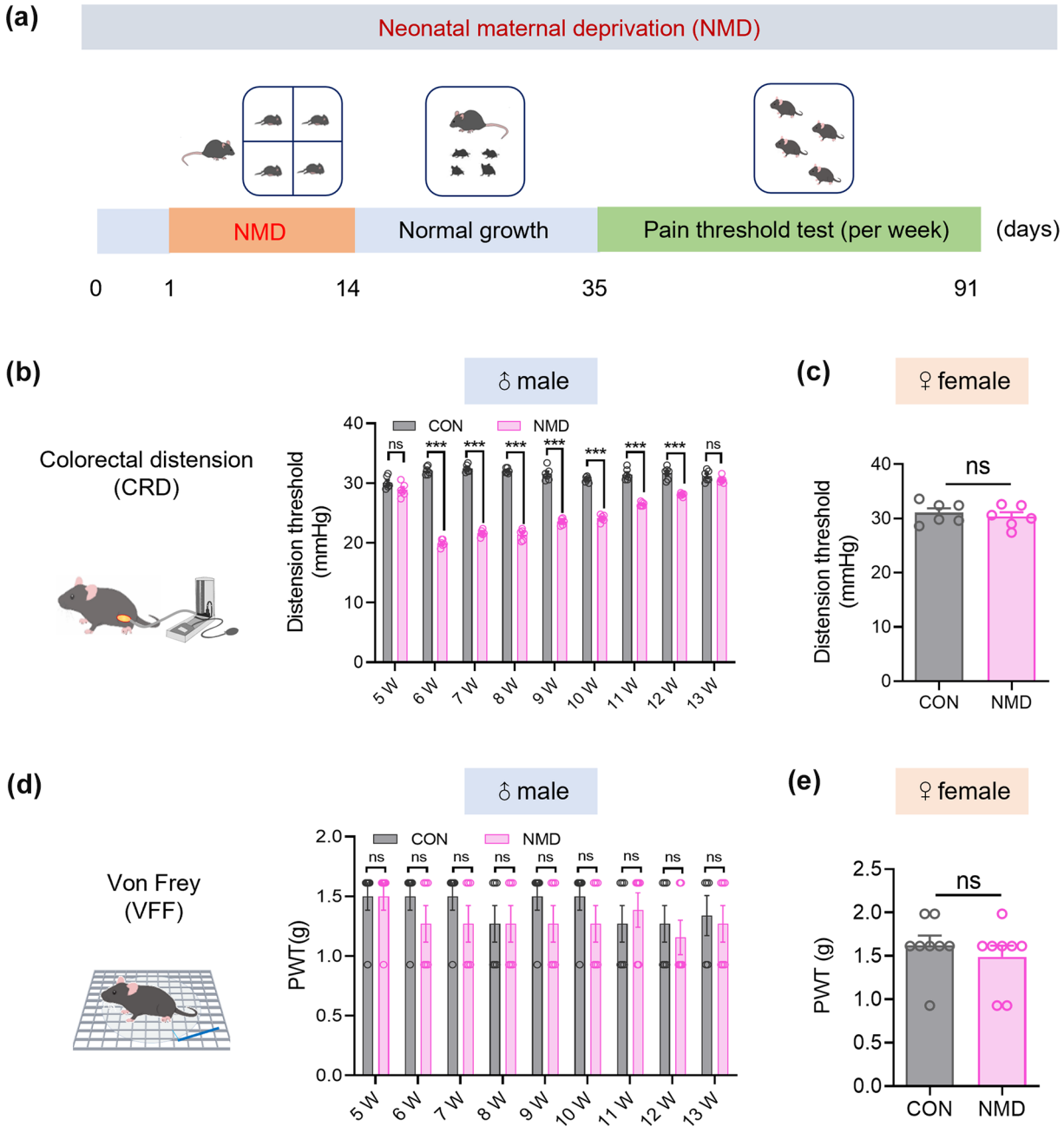

Figure 1. NMD induced chronic visceral but not somatic pain in male mice. (a) Timeline of modeling and pain threshold detection in the NMD model. (b) Schematic of CRD for evaluating visceral pain in mice (left), CRD thresholds of NMD and CON male mice at 5–13 weeks of age (right, $n = 6$, $^{***}p < 0.001$, two-way ANOVA). (c) CRD thresholds of NMD and CON female mice at 6 weeks of age ($n = 6$, Student's *t*-test). (d) Schematic of the Von Frey mechanical stimulation (left), paw withdrawal thresholds in NMD and CON male mice at 5–13 weeks of age (right, $n = 6$, two-way ANOVA). (e) Paw withdrawal thresholds in NMD and CON female mice at 6 weeks of age ($n = 8$, Student's *t*-test).

To investigate the expression of LRRC8A in the ACC of female mice, we conducted qPCR and western blotting. There was no significant difference in the relative mRNA expression of LRRC8A in the ACC of CON and NMD female mice (Figure 2(f), $n = 4$, Student's *t*-test). Similarly, there was no significant difference in the protein expression of LRRC8A between the two groups of mice (Figure 2(g), $n = 6$, Student's *t*-test). It indicated that the upregulation of LRRC8A expression in NMD mice was sex-specific. These suggest that the upregulation of LRRC8A expression in NMD mice is brain-region and sex-specific.

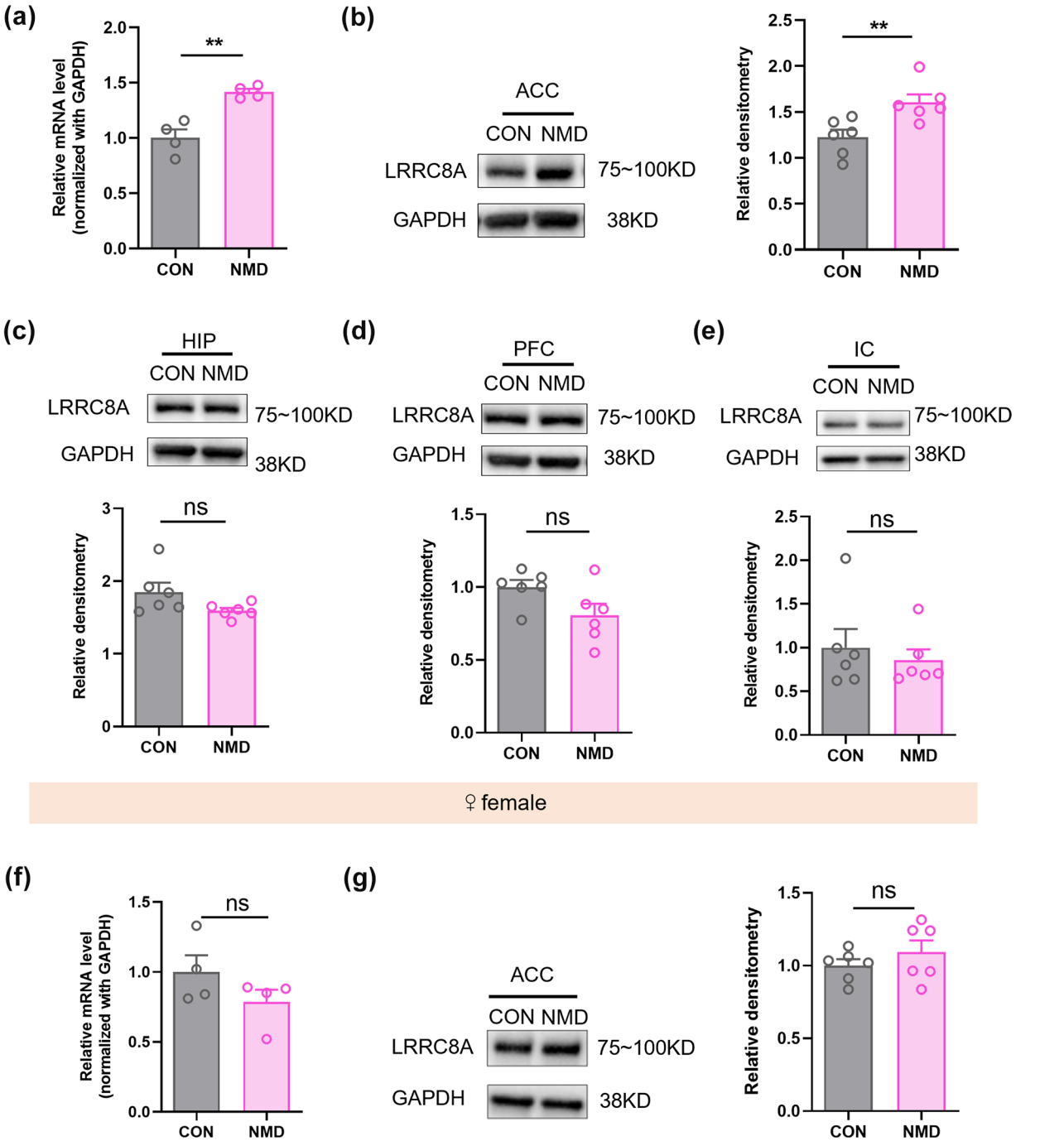

Figure 2. LRRC8A expression levels were significantly elevated in the ACC of NMD male mice, whereas there were no significant changes in LRRC8A expression in the ACC of NMD female mice. (a) Statistical graph of changes in LRRC8A mRNA expression in ACC of CON and NMD male mice detected by qPCR ($n = 4$, $^{**}p < 0.01$, Student's *t*-test). (b) Representative western blotting of LRRC8A and GAPDH in the ACC of CON and NMD male mice (left). Quantification of LRRC8A protein levels in ACC of CON and NMD male mice (right, $n = 6$, $^{**}p < 0.01$, Student's *t*-test). (c) Representative western blotting of LRRC8A and GAPDH in the HIP of CON and NMD male mice, and quantification of LRRC8A protein levels in HIP of CON and NMD male mice ($n = 6$, Student's *t*-test). (d) Representative western blotting of LRRC8A and GAPDH in the PFC of CON and NMD male mice, and quantification of LRRC8A protein levels in the PFC of CON and NMD male mice ($n = 6$, Student's *t*-test). (e) Representative western blotting of LRRC8A and GAPDH in the IC of CON and NMD male mice, and quantification of LRRC8A protein levels in the IC of CON and NMD male mice ($n = 6$, Student's *t*-test). (f) Expression changes of LRRC8A mRNA in the ACC of CON and NMD female mice detected by qPCR ($n = 4$, Student's *t*-test). (g) Representative western blotting of LRRC8A and GAPDH in ACC of CON and NMD female mice, and quantification of LRRC8A protein levels in ACC of CON and NMD female mice ($n = 6$, Student's *t*-test).
HIP: hippocampus; IC: insular cortex; PFC: prefrontal cortex.

LRRC8A co-localized mainly with neurons in the ACC

To identify the cell types expressing LRRC8A in the ACC, paraffin section and immunofluorescence staining were performed, and the staining results were shown in Figure 3(a). Statistical results revealed that the rate of LRRC8A-positive cells in the ACC of NMD mice was significantly higher than that of CON mice. Furthermore, the ratio of positive cells co-localized with NeuN was elevated in both CON and NMD mice, with a significantly greater proportion in NMD mice. In contrast, the ratio of positive cells co-localized with Iba1 and GFAP was lower for LRRC8A and showed no significant difference between the two groups (Figure 3(b) and (c), $n=6$, $^{***}p<0.001$, Student's *t*-test). The results indicated that the expression of LRRC8A was significantly upregulated in the ACC of NMD mice, consistent with earlier western blotting results. In the ACC of both CON and NMD mice, LRRC8A was primarily co-localized with NeuN, while only a small number of LRRC8A-positive cells were co-localized with Iba1 and GFAP.

LRRC8A inhibitor DCPIB significantly alleviated chronic visceral pain in NMD mice

To further verify the role of LRRC8A in chronic visceral pain in NMD mice, DCPIB, an inhibitor of LRRC8A, was microinjected into the ACC. The timeline of this experiment, the placement of the administration cannula, and a schematic representation of the administration sites was shown in Figure 4(a). The single-injection administration was performed to determine the optimal delivery concentration of DCPIB at different concentrations (DMSO, 10, 20, 50, and 100 μM) into the ACC of NMD mice, respectively. Compared with DMSO injections, injections of 10, 20, 50, and 100 μM DCPIB significantly upregulated the CRD threshold to a specific time frame. Notably, the 20 μM concentrations produced the most significant upregulation and sustained efficacy for up to 7 h, suggesting that 20 μM DCPIB was the most effective in alleviating chronic visceral pain in the NMD mice (Figure 4(b), $n=6$, $^{*}p<0.05$, $^{**}p<0.01$, $^{***}p<0.001$, two-way ANOVA). We also considered the potency and toxicity of the drug, choosing 20 μM DCPIB as the optimal administration concentration for subsequent related experiments. To investigate the effects of multiple administrations on the duration of efficacy, we administered DCPIB into the ACC of NMD mice for seven consecutive days. It was found that the CRD thresholds receiving 20 μM DCPIB were significantly elevated from 0.5 to 12 h after the last administration, indicating that the efficacy range was enhanced with multiple administrations of DCPIB (Figure 4(c), $n=6$, $^{***}p<0.001$, two-way ANOVA).

To assess whether DCPIB would affect CON mice, 1 μL DMSO or 20 μM DCPIB was injected into the ACC of CON mice in a single injection and the CRD thresholds were examined at different time points. There was no significant difference in CRD thresholds between the two groups, indicating that DCPIB did not affect the CRD thresholds in CON mice (Figure 4(d), $n=6$, two-way ANOVA). These results suggest that DCPIB significantly alleviated chronic visceral pain in NMD mice while having no significant effect on pain thresholds in CON mice, thereby demonstrating the regulatory role of LRRC8A in chronic visceral pain of NMD mice.

The ATP concentration was significantly upregulated in the ACC of NMD male mice

It has been shown that LRRC8A mediated the increased release of ATP, which promotes the development of chronic neuropathic pain.[45] Therefore, we aimed to explore whether LRRC8A was involved in the regulation of chronic visceral pain through ATP release. The schematic of the ATP concentration test of CON and NMD male mice was shown in Figure 5(a). The data showed that ATP concentration was significantly upregulated in the ACC of NMD mice compared to CON mice (Figure 5(b), $n=6$, $^{*}p<0.05$, Student's *t*-test). Moreover, we observed a significant decrease in ATP concentration after inhibiting LRRC8A in the ACC (Figure 5(c) and (d), $n=6$, $^{*}p<0.05$, Student's *t*-test). This suggests that the upregulation of LRRC8A in the ACC of NMD mice may play a role in regulating chronic visceral pain through the ATP release.

The increased ATP may interact with purinergic receptors, therefore, the expression of purinergic receptors was examined. Our results revealed that the mRNA expression levels of P2X4Rs were significantly upregulated in the ACC regions of NMD mice compared to CON mice (Figure 5(e), $n=4$, $^{*}p<0.05$, Student's *t*-test). In contrast, the mRNA expression levels of P2X1R, P2X2R, P2X3R, P2X5R, P2X6R, and P2X7R in the ACC showed no significant difference between the CON and NMD groups (Figure 5(f–k), $n=4$, Student's *t*-test). Next, protein level of P2X4Rs was examined, and it was found that there was no significant difference in their expression in the ACC between CON and NMD mice (Figure 5(l), $n=6$, Student's *t*-test). The expression of P2YRs was assessed using the same method, revealing that the mRNA expression level of P2Y12R was significantly upregulated in the ACC of NMD mice compared to CON mice (Figure 5(m), $n=4$, $^{*}p<0.05$, Student's *t*-test). In contrast, the mRNA expression levels of P2Y1R, P2Y2R, P2Y4R, P2Y6R, P2Y13R, and P2Y14R showed no significant difference between the CON and NMD groups (Figure 5(n–s), $n=4$, Student's *t*-test). Similarly, protein levels of P2Y12R were examined, and there was no significant difference in their expression in the ACC between CON and NMD mice (Figure 5(t), $n=6$, Student's *t*-test).

The above results indicate that the upregulated expression of LRRC8A in the ACC of NMD mice may play a role in regulating chronic visceral pain by mediating ATP release. However, we found no significant differences in the protein

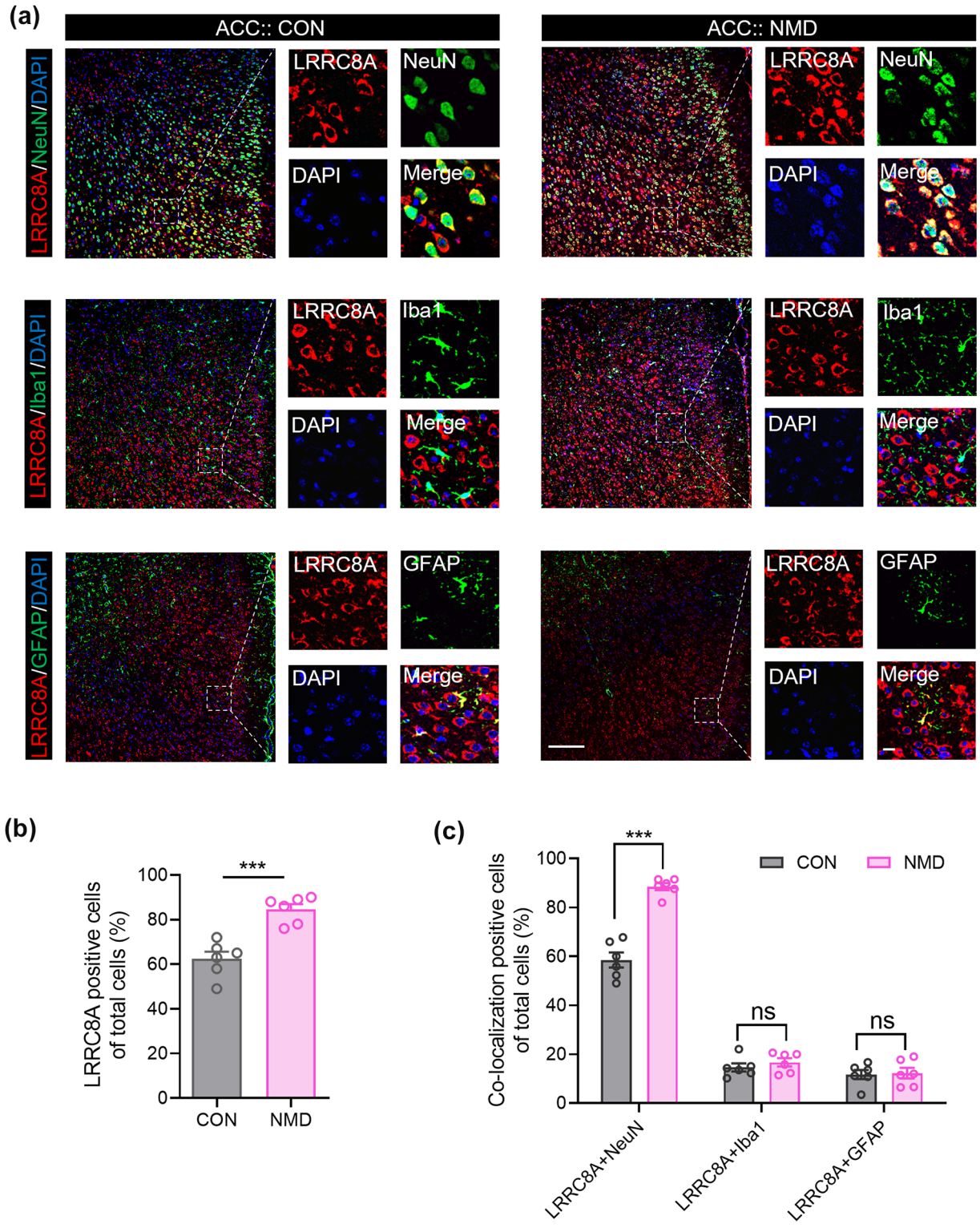

Figure 3. NMD increased the proportion of LRRC8A-positive cells in the ACC of male mice, and LRRC8A was predominantly expressed in ACC neurons. (a) Representative immunofluorescence images of LRRC8A (red), NeuN (green), Iba1 (green), GFAP (green), and DAPI (blue) expression in the brain regions of the ACC in CON and NMD male mice, respectively, on the left side of the respective group of the figure (Scale bar = 100 μm), and the right side of the respective group is the area shown by white box magnification (Scale bar = 20 μm), which allows a clearer view of the co-localization of protein expression. (b) The statistics of the number of LRRC8A-positive cells of the total number of cells in the ACC of CON and NMD male mice ($n = 6$, ***$p < 0.001$, Student's *t*-test). (c) The analysis of the co-localization ratio of LRRC8A with NeuN, Iba1, and GFAP ($n = 6$, ***$p < 0.001$, Student's *t*-test).

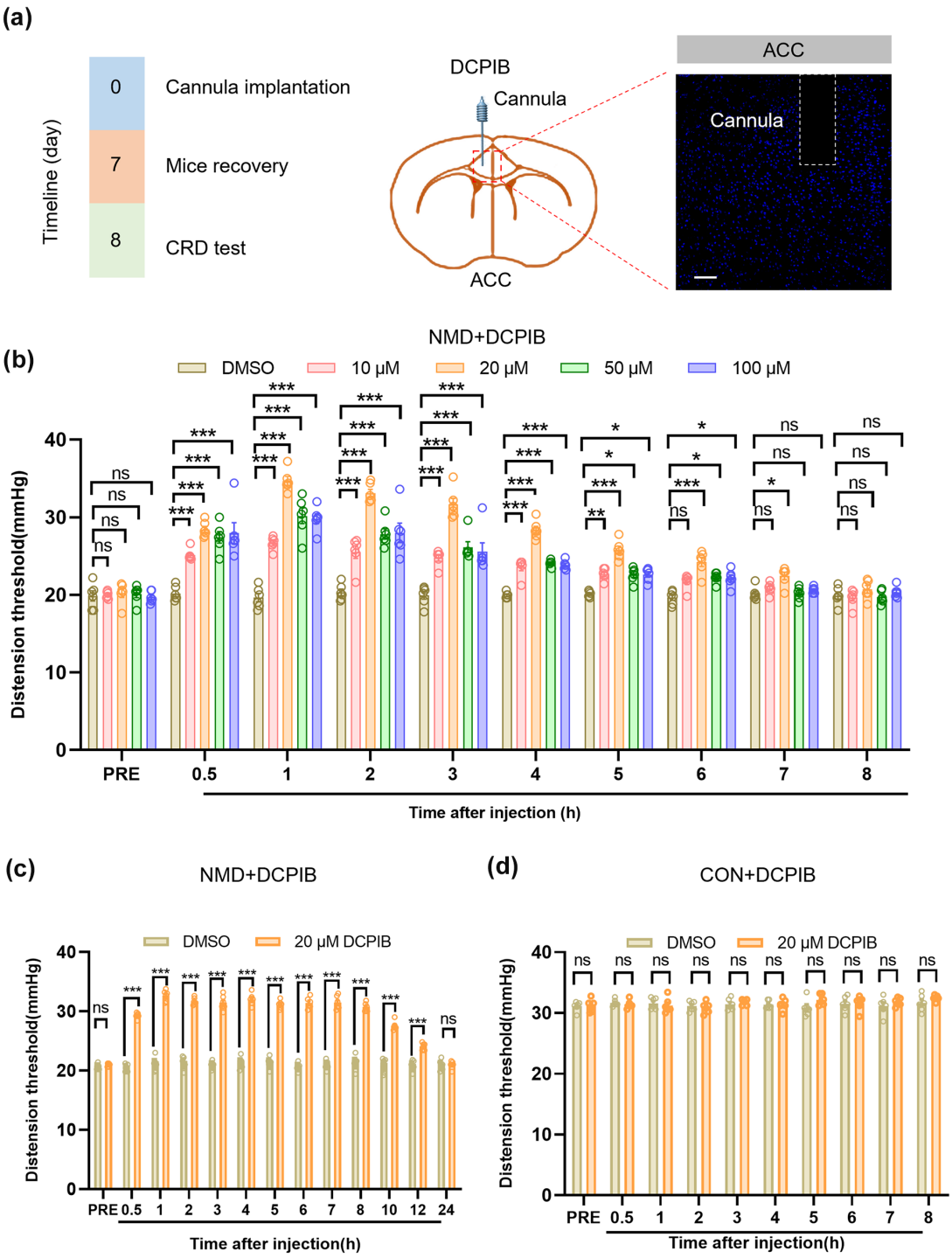

Figure 4. Intra-ACC microinjection of DCPIB alleviated visceral pain sensitization in NMD male mice but did not affect visceral pain sensitization in CON male mice. (a) Timeline of experiments using brain stereotaxic device for microdosing into ACC brain region and pain behavior detection (left), schematic diagram of ACC with buried drug delivery cannula and microinjection of DCPIB (middle), and representative images of drug delivery site after buried drug delivery cannula in ACC (right, Scale bar = 100 μm). (b) Statistical graph of CRD thresholds in NMD mice detected before and after single injection of 1 μL of DCPIB at different concentrations (DMSO, 10, 20, 50, and 100 μM) at different time points ($n = 6$, $^{*}p < 0.05$, $^{**}p < 0.01$, $^{***}p < 0.001$, 10, 20, 50, and 100 μM groups at each time point were compared with the DMSO group, two-way ANOVA). (c) Statistical graph of CRD thresholds in NMD mice detected before and after injection of DCPIB at 20 μM concentration for seven consecutive days at different time points ($n = 6$, $^{***}p < 0.001$, two-way ANOVA). (d) Statistical graph of CRD thresholds in CON mice detected before and after single injection of 1 μL DMSO or DCPIB at 20 μM concentration at different time points. ($n = 6$, two-way ANOVA).

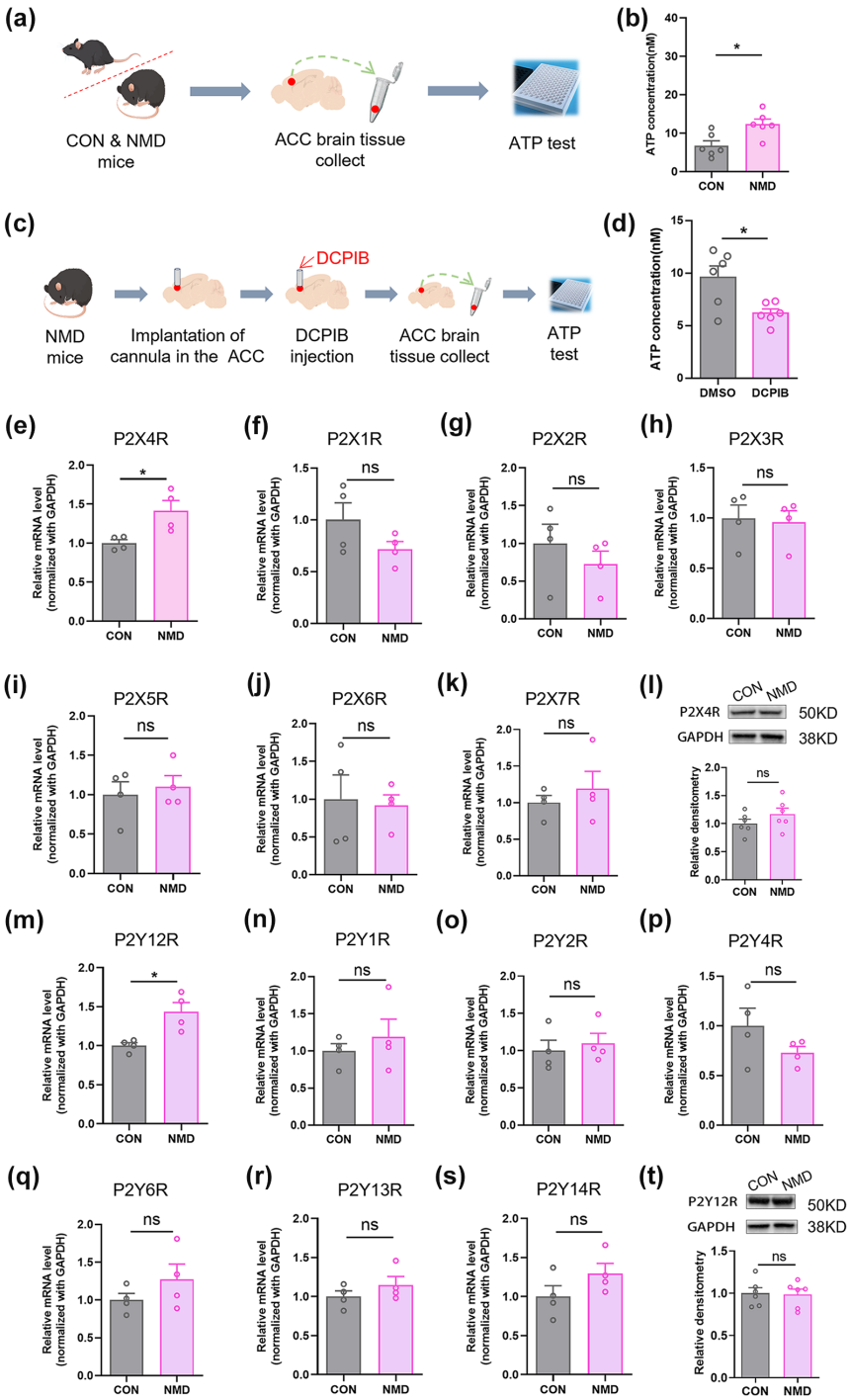

Figure 5. ATP concentration was significantly up regulated in the ACC of NMD male mice, whereas there was no significant difference in the protein expression levels of purinergic receptors. (a) Schematic diagram of sampling process of the ACC and ATP test. (b) Statistical graph of ATP concentration test in the ACC of CON and NMD male mice ($n = 6$, $^*p < 0.05$, Student's *t*-test). (c) Schematic diagram of sampling process of ACC and ATP test in NMD mice. (d) Statistical graph of ATP concentration test in the ACC of DMSO and DCPIB group ($n = 6$, $^*p < 0.05$, Student's *t*-test). (e–k) Statistical graphs of mRNA expression changes of P2X4R(e), P2X1R(f), P2X2R(g), P2X3R(h), P2X5R(i), P2X6R(j), and P2X7R(k) in CON and NMD male mice ACC by qPCR ($n = 4$, $^*p < 0.05$, Student's *t*-test). (l) Representative western blotting of P2X4R and GAPDH in ACC of CON and NMD male mice, and quantification of P2X4R protein levels in ACC of CON and NMD male mice ($n = 6$, Student's *t*-test). (m–s) Statistical graphs of mRNA expression changes of P2Y12R(m), P2Y1R(n), P2Y2R(o), P2Y4R(p), P2Y6R(q), P2Y13R(r), and P2Y14R(s) in ACC of CON and NMD male mice by qPCR ($n = 4$, $^*p < 0.05$, Student's *t*-test). (t) Representative western blotting of P2Y12R and GAPDH in ACC of CON and NMD male mice, and quantification of P2Y12R protein levels in ACC of CON and NMD male mice ($n = 6$, Student's *t*-test).

expression of purinergic receptors in the ACC of NMD mice. This suggests that the increased release of ATP in the ACC may be transported to other brain regions to exert its effects.

LRRC8A was not differentially expressed in the ACC of CFA mice

To investigate whether LRRC8A was involved in other pain models, we induced a somatic pain model by injecting CFA into the left hind paw of adult male mice, with an equal number of NS-injected serving as the control group. It was found that there was significant redness and swelling in the hind limbs of mice in the CFA group compared to the NS group, as schematically shown in Figure 6(a). To assess the success of modeling, the paw withdrawal frequency of mice was tested by von Frey mechanical stimulation. The paw withdrawal frequency was significantly upregulated in CFA-injected mice compared to NS-injected mice, indicating that somatic hyperalgesia was successfully induced following the plantar injection of CFA (Figure 6(b), $n=6$, $^{***}p<0.001$, Student's *t*-test). Subsequently, we examined the changes in LRRC8A expression in the ACC of NS and CFA mice. qPCR results indicated no significant difference in the mRNA expression of LRRC8A in the ACC between the two groups (Figure 6(c), $n=4$, Student's *t*-test). Additionally, western blotting analysis revealed no significant differences in the protein expression of LRRC8A in the ACC of the two groups (Figure 6(d), $n=6$, Student's *t*-test). We detected the ATP concentration in the ACC of CFA mice and found no significant difference compared to the NS group (Figure 6(e and f), $n=6$, Student's *t*-test). These findings suggest that LRRC8A is not involved in CFA-induced somatic pain and may be model-specific.

Discussion

The increasing evidence highlights that central mechanisms play a significant role in chronic visceral pain, yet the underlying molecular mechanisms in the brain remain poorly understood. This study demonstrates that the ion channel LRRC8A is highly expressed in the ACC of NMD male mice. Furthermore, targeted injection of an LRRC8A inhibitor into this specific brain region significantly alleviates visceral pain. These findings offer new insights into the central mechanisms of visceral pain and suggest potential therapeutic targets for IBS.

One of the most important findings is that new ion channels play a critical regulatory role in chronic visceral pain. A previous study found that protein expression of acid-sensing ion channel 1 (ASIC1) and sodium-potassium-chloride cotransporter protein 1 (NKCC1) was significantly upregulated in the dorsal horn of the spinal cord of NMD rats and that the ASIC1-NKCC1 signaling pathway was involved in the regulation of chronic visceral pain in NMD rats.[60] It has also been shown that NMD enhances visceral hypersensitivity in the spinal cord, thoracic, lumbar spine, and lumbosacral segments and increases the expression of P2X4 receptors (a family of ATP-gated non-selective cation channels) in rats.[61] Evidence for the involvement of purinergic receptors, a family of ion channels, in the regulation of chronic visceral pain is growing, but mostly focused on the spinal cord.[62–64] However, the mechanisms related to the involvement of ion channels in the regulation of chronic visceral pain in the brain are unclear. Our study uniquely identified LRRC8A, a volume-regulated anion channel, as playing a regulatory role in chronic visceral pain in the ACC of NMD male mice. We propose that LRRC8A may regulate chronic visceral pain by mediating the ATP release. Additionally, our findings indicate that the expression of LRRC8A is somewhat brain-region specific, sex-specific, and model-specific.

In this study, we chose the well-established neonatal maternal deprivation (NMD) model to induce visceral pain.[18] Our data demonstrate that NMD induced chronic visceral pain without affecting somatic pain in male mice, ruling out the influence of other pain types on the chronic visceral pain findings in this model. Moreover, NMD did not induce chronic visceral pain in female mice. There were no significant differences in the expression of LRRC8A at both mRNA and protein levels in the ACC of CON and NMD female mice. This suggests that the expression of LRRC8A exhibits a degree of sex-specificity in the context of chronic visceral pain. This result is supported by previous reports that the physiological cycle of female mice and their estrogen affect the assessment of visceral pain behavior.[65] Therefore, we used male mice as the subjects in this study. Additionally, our results indicate that LRRC8A is not involved in CFA-induced somatic pain with model specificity. Notably, we found that the expression of LRRC8A at both mRNA and protein levels was upregulated in the ACC of NMD male mice, whereas there was no significant difference in the pain-related HIP, PFC, and IC. This suggests that the expression of LRRC8A exhibits a degree of brain-region specificity.

A previous study showed that LRRC8A is primarily expressed on spinal microglia, regulating neuropathic pain.[45] In contrast, our study found that LRRC8A is mainly expressed on neurons in the ACC. It indicates that LRRC8A plays an important regulatory role in chronic visceral pain in IBS patients and has its unique regulatory mechanism. Consistently, we observed increased ATP release in the ACC, suggesting that LRRC8A may be involved in chronic visceral pain by regulating ATP release. In the next study, we will validate this hypothesis through further experiments. ATP is released and binds to purinergic receptors, thereby exerting its effects. Interestingly, our results showed no significant difference in the expression of purinergic receptors at the protein level in the ACC of NMD mice, suggesting that the increased release of ATP in the ACC regions of NMD mice may be transported to other brain regions to play a role. Although we did not continue to explore the mechanism in this study, we will further explore the mechanism of ATP

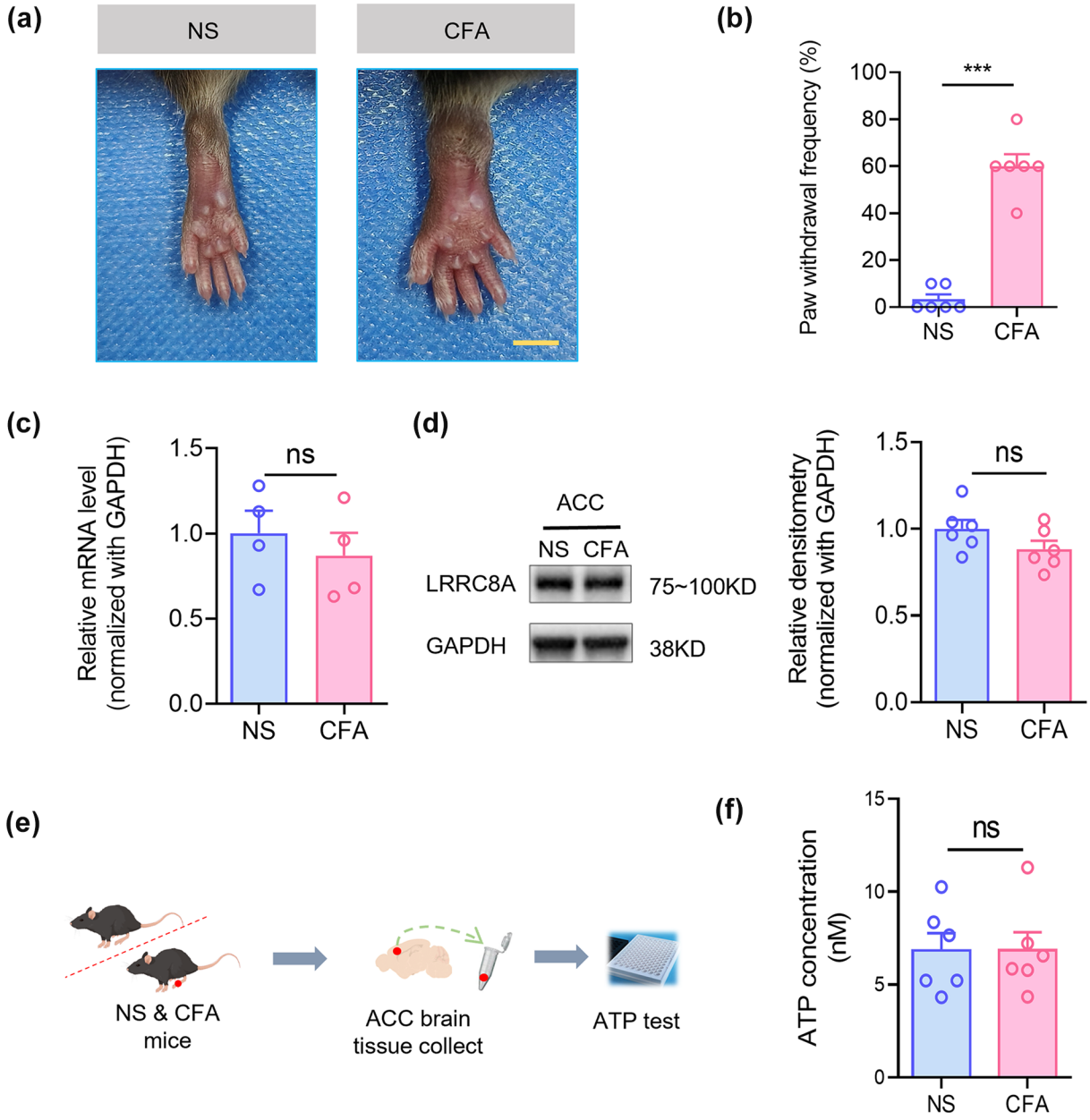

Figure 6. No significant difference in protein expression levels of LRRC8A in ACC of mice with CFA-induced somatic hyperalgesia. (a) Schematic diagrams of mice after NS injection in the left hind paw (left), and after injection of CFA in the left hind paw (right). (b) Statistical graph of the paw withdrawal frequency in NS and CFA mice after modeling ($n = 6$, $^{***}p < 0.001$, Student's *t*-test). (c) Statistical graph of changes in LRRC8A mRNA expression in the ACC of NS and CFA mice ($n = 4$, Student's *t*-test). (d) Left: representative western blotting of LRRC8A and GAPDH in the ACC of NS and CFA mice. Right: quantification of LRRC8A protein levels in the ACC of NS and CFA mice ($n = 6$, Student's *t*-test). (e) Schematic diagram of sampling process of the ACC and ATP test. (f) Statistical graph of ATP concentration test in the ACC of CON and NMD male mice ($n = 6$, Student's *t*-test).

release and the related neural circuit in our next research work. In addition, the inhibitors of LRRC8A were injected into the right ACC of mice. Previous studies have shown that unilateral injection administration of DCPIB causes relatively less damage to the animals while remaining equally effective compared to bilateral injections in the ACC,[66] a finding supported by our results.

In summary, our study indicates that in the ACC of NMD male mice, the ion channel LRRC8A, primarily expressed on neurons, may regulate chronic visceral pain through the release of ATP (Figure 7). These findings highlight a novel mechanism by which the ACC regulates chronic visceral pain and suggest LRRC8A as a potential target for treating chronic visceral pain in IBS patients.

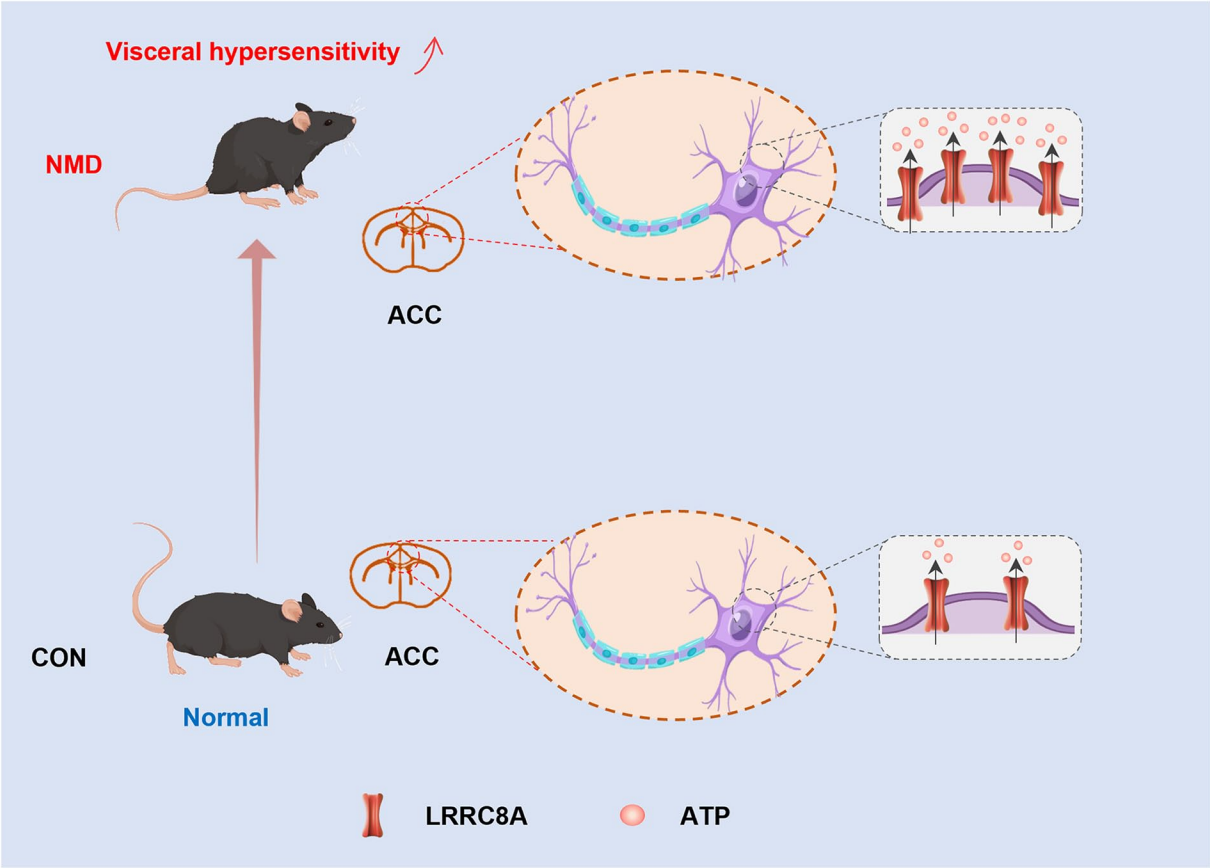

Figure 7. A working model of this study. Compared with CON mice, NMD mice produce visceral hypersensitivity and have significantly increased expression of LRRC8A on neurons in the ACC, which mediates increased release of ATP to participate in the regulation of chronic visceral pain.

Author contributions

J-N. L performed experiments, analyzed data, and prepared the manuscript. J-H. D, Z-L.Y, and L. L analyzed data and prepared the figures. X-L. B and F-C. Z analyzed data and revised the manuscript. G-Y. X designed and supervised the experiments and finalized the manuscript. All the authors have read and approved the paper.

Declaration of conflicting interests

The author(s) declared no potential conflicts of interest with respect to the research, authorship, and/or publication of this article.

Funding

The author(s) disclosed receipt of the following financial support for the research, authorship, and/or publication of this article: This work was supported by grants from the National Natural Science Foundation of China (32230041 and 81920108016), the Chinese Red Cross Foundation National Brain Nutrition Research Fund, and the Priority Academic Program Development of Jiangsu Higher Education Institutions of China. The funders had no role in the study design, data collection and analysis, decision to publish, or preparation of the manuscript.

ORCID iDs

Jin-Nan Lu https://orcid.org/0009-0003-8138-5124
Guang-Yin Xu https://orcid.org/0000-0002-5495-4120

References

1. Jiang B-C, Liu T, Gao Y-J. Chemokines in chronic pain: cellular and molecular mechanisms and therapeutic potential. *Pharmacol Ther* 2020; 212: 107581.
2. Xu Q-Y, Zhang H-L, Du H, Li Y-C, Ji F-H, Li R, Xu G-Y. Identification of a glutamatergic claustrum-anterior cingulate cortex circuit for visceral pain processing. *J Neurosci* 2022; 42: 8154–8168.
3. Grundy L, Erickson A, Brierley SM. Visceral pain. *Annu Rev Physiol* 2019; 81: 261–284.
4. Long J-Y, Wang X-J, Li X-Y, Kong X-H, Yang G, Zhang D, Yang Y-T, Shi Z, Ma X-P. Spinal microglia and astrocytes: two key players in chronic visceral pain pathogenesis. *Neurochem Res* 2021; 47: 545–551.
5. Yi Z-L, Lu J-N, Zhu J-J, He T-T, Xu Y-R, Huang Z-W, Li Y-C, Xu G-Y. Upregulation of KDM6B in the anterior cingulate cortex contributes to neonatal maternal deprivation-induced chronic visceral pain in mice. *Mol Pain* 2024; 20: 17448069241260349.

6. Weng R-X, Wei Y-X, Li Y-C, Xu X, Zhuang J-B, Xu G-Y, Li R. Folic acid attenuates chronic visceral pain by reducing clostridiales abundance and hydrogen sulfide production. *Mol Pain* 2023; 19: 17448069221149834.
7. Brierley SM, Grundy L, Castro J, Harrington AM, Hannig G, Camilleri M. Guanylate cyclase-C agonists as peripherally acting treatments of chronic visceral pain. *Trends Pharmacol Sci* 2022; 43: 110–122.
8. Di Rosa C, Altomare A, Terrigno V, Carbone F, Tack J, Cicala M, Guarino M. Constipation-predominant Irritable Bowel Syndrome (IBS-C): effects of different nutritional patterns on intestinal dysbiosis and symptoms. *Nutrients* 2023; 15: 1647.
9. Mayer EA, Ryu HJ, Bhatt RR. The neurobiology of irritable bowel syndrome. *Mol Psychiatry* 2023; 28: 1451–1465.
10. Johnson AC, Farmer AD, Ness TJ, Greenwood-Van Meerveld B. Critical evaluation of animal models of visceral pain for therapeutics development: a focus on irritable bowel syndrome. *Neurogastroenterol Motil* 2019; 32: 13776.
11. Ford AC, Vanner S, Kashyap PC, Nasser Y. Chronic visceral pain: new peripheral mechanistic insights and resulting treatments. *Gastroenterology* 2024; 166: 976–994.
12. Zhou Q, Verne GN. Epigenetic modulation of visceral nociception. *Neurogastroenterol Motil* 2022; 34: 14443.
13. Li D, Du H, Qu ST, Wu JL, Li YC, Xu QY, Chen X, Dai XX, Xu JT, Wang Q, Xu GY. Thalamic nucleus reuniens glutamatergic neurons mediate colorectal visceral pain in mice via 5-HT(2B) receptors. *Neurosci Bull* 2024; 40: 1421–1433.
14. Chen Z, Zhou T, Zhang Y, Dong H, Jin W. Mast cells in the paraventricular nucleus participate in visceral hypersensitivity induced by neonatal maternal separation. *Behav Brain Res* 2021; 402: 113113.
15. Wu K, Gao J-h, Hua R, Peng X-h, Wang H, Zhang Y-m. Predisposition of neonatal maternal separation to visceral hypersensitivity via downregulation of small-conductance calcium-activated potassium channel subtype 2 (SK2) in mice. *Neural Plast* 2020; 2020: 1–15.
16. Chang X, Zhang H, Chen S. Neural circuits regulating visceral pain. *Commun Biol* 2024; 7: 457.
17. Császár-Nagy N, Bókkon I. Hypnotherapy and IBS: implicit, long-term stress memory in the ENS? *Heliyon* 2023; 9: e12751.
18. Li YC, Wang Q, Li MG, Hu SF, Xu GY. A paraventricular hypothalamic nucleus input to ventral of lateral septal nucleus controls chronic visceral pain. *Pain* 2023; 164: 625–637.
19. Petitfils C, Maurel S, Payros G, Hueber A, Agaiz B, Gazzo G, Marrocco R, Auvray F, Langevin G, Motta JP, Floch P, Tremblay-Franco M, Galano JM, Guy A, Durand T, Lachambre S, Durbec A, Hussein H, Decraecker L, Bertrand-Michel J, Saoudi A, Oswald E, Poisbeau P, Dietrich G, Melchior C, Boeckxstaens G, Serino M, Le Faouder P, Cenac N. Identification of bacterial lipopeptides as key players in IBS. *Gut* 2023; 72: 939–950.
20. Monosov IE, Haber SN, Leuthardt EC, Jezzini A. Anterior cingulate cortex and the control of dynamic behavior in primates. *Curr Biol* 2020; 30: R1442–R1454.
21. Chen Q-Y, Li X-H, Zhuo M. NMDA receptors and synaptic plasticity in the anterior cingulate cortex. *Neuropharmacology* 2021; 197: 108749.
22. Journée SH, Mathis VP, Fillinger C, Veinante P, Yalcin I. Janus effect of the anterior cingulate cortex: pain and emotion. *Neurosci Biobehav Rev* 2023; 153: 105362.
23. Seamans JK, Floresco SB. Event-based control of autonomic and emotional states by the anterior cingulate cortex. *Neurosci Biobehav Rev* 2022; 133: 104503.
24. Rolls ET. Emotion, motivation, decision-making, the orbitofrontal cortex, anterior cingulate cortex, and the amygdala. *Brain Struct Funct* 2023; 228: 1201–1257.
25. Jee HJ, Zhu E, Sun M, Liu W, Zhang Q, Wang J. Anterior cingulate cortex regulates pain catastrophizing-like behaviors in rats. *Mol Brain* 2023; 16: 71.
26. Zhang TT, Guo SS, Wang HY, Jing Q, Yi X, Hu ZH, Yu XR, Xu TL, Liu MG, Zhao X. An anterior cingulate cortex-to-midbrain projection controls chronic itch in mice. *Neurosci Bull* 2023; 39: 793–807.
27. Peng B, Wu XB, Zhang ZJ, Cao DL, Zhao LX, Wu H, Gao YJ. Anterior cingulate cortex contributes to the hyperlocomotion under nitrogen narcosis. *Neurosci Bull*. Epub ahead of print 19 August 2024. DOI: 10.1007/s12264-024-01278-z.
28. Wei J, Li L, Zhang J, Shi E, Yang J, Liu X. Computational modeling of the prefrontal-cingulate cortex to investigate the role of coupling relationships for balancing emotion and cognition. *Neurosci Bull* 2025; 41: 33–45.
29. Zhang L, Cheng Y, Xue Z, Wu S, Qiu Z, Jiang H. Comparative molecular taxonomics of neuron in cingulate cortex of rhesus monkey and mouse via single-nucleus RNA sequencing. *Neurosci Bull* 2024; 40: 1751–1756.
30. Valentinova K, Acuña MA, Ntamati NR, Nevian NE, Nevian T. An amygdala-to-cingulate cortex circuit for conflicting choices in chronic pain. *Cell Rep* 2023; 42: 113125.
31. Duan Y, Li Q, Zhou Y, Chen S, Li Y, Zang Y. Activation of the TNF-α-necroptosis pathway in parvalbumin-expressing interneurons of the anterior cingulate cortex contributes to neuropathic pain. *Int J Mol Sci* 2023; 24: 15454.
32. Moon HC, Park YS. Optogenetic stimulation of the anterior cingulate cortex modulates the pain processing in neuropathic pain: a review. *J Mol Neurosci* 2021; 72: 1–8.
33. Wu J, Hua L, Liu W, Yang X, Tang X, Yuan S, Zhou S, Ye Q, Cui S, Wu Z, Lai L, Tang C, Wang L, Yi W, Yao L, Xu N. Electroacupuncture exerts analgesic effects by restoring hyperactivity via cannabinoid type 1 receptors in the anterior cingulate cortex in chronic inflammatory pain. *Mol Neurobiol* 2023; 61: 2949–2963.
34. Xiao X, Ding M, Zhang Y-Q. Role of the anterior cingulate cortex in translational pain research. *Neurosci Bull* 2021; 37: 405–422.
35. Song Z-h, Song X-J, Yang C-l, Cao P, Mao Y, Jin Y, Xu M-y, Wang H-t, Zhu X, Wang W, Zhang Z, Tao W-j. Up-regulation of microglial chemokine CXCL12 in anterior cingulate cortex mediates neuropathic pain in diabetic mice. *Acta Pharmacol Sin* 2023; 44: 1337–1349.
36. Zhou J-J, Luo Y, Chen S-R, Shao J-Y, Sah R, Pan H-L. LRRC8A-dependent volume-regulated anion channels contribute to ischemia-induced brain injury and glutamatergic input to hippocampal neurons. *Exp Neurol* 2020; 332: 113391.
37. Jeon D, Ryu K, Jo S, Kim I, Namkung W. VI-116, a novel potent inhibitor of VRAC with minimal effect on ANO1. *Int J Mol Sci* 2022; 23: 5168.
38. Zuccolini P, Ferrera L, Remigante A, Picco C, Barbieri R, Bertelli S, Moran O, Gavazzo P, Pusch M. The VRAC blocker DCPIB directly gates the BK channels and increases intracellular Ca2+ in melanoma and pancreatic duct adenocarcinoma cell lines. *Br J Pharmacol* 2022; 179: 3452–3469.

39. Friard J, Corinus A, Cougnon M, Tauc M, Pisani DF, Duranton C, Rubera I. LRRC8/VRAC channels exhibit a noncanonical permeability to glutathione, which modulates epithelial-to-mesenchymal transition (EMT). *Cell Death Dis* 2019; 10: 925.
40. Han Q, Liu S, Li Z, Hu F, Zhang Q, Zhou M, Chen J, Lei T, Zhang H. DCPIB, a potent volume-regulated anion channel antagonist, attenuates microglia-mediated inflammatory response and neuronal injury following focal cerebral ischemia. *Brain Res* 2014; 1542: 176–185.
41. Ghouli MR, Fiacco TA, Binder DK. Structure-function relationships of the LRRC8 subunits and subdomains of the volume-regulated anion channel (VRAC). *Front Cell Neurosci* 2022; 16: 962714.
42. Kern DM, Oh S, Hite RK, Brohawn SG. Cryo-EM structures of the DCPIB-inhibited volume-regulated anion channel LRRC8A in lipid nanodiscs. *eLife* 2019; 8: 42636.
43. Ding Y, Hu L, Wang X, Sun Q, Hu T, Liu J, Shen D, Zhang Y, Chen W, Wei C, Liu M, Liu D, Wang P, Zhang C, Zhang J, Li Q, Yang F. The contribution of spinal dorsal horn astrocytes in neuropathic pain at the early stage of EAE. *Neurobiol Dis* 2022; 175: 105914.
44. Furuya K, Hirata H, Kobayashi T, Sokabe M. Sphingosine-1-phosphate induces ATP release via volume-regulated anion channels in breast cell lines. *Life* 2021; 11: 851.
45. Chu J, Yang J, Zhou Y, Chen J, Chen KH, Zhang C, Cheng HY, Koylass N, Liu JO, Guan Y, Qiu Z. ATP-releasing SWELL1 channel in spinal microglia contributes to neuropathic pain. *Sci Adv* 2023; 9: eade9931.
46. Yang R, Yang J, Li Z, Su R, Zou L, Li L, Xu X, Li G, Liu S, Liang S, Xu C. Pinocembrin inhibits P2X4 receptor-mediated pyroptosis in hippocampus to alleviate the behaviours of chronic pain and depression comorbidity in rats. *Mol Neurobiol* 2022; 59: 7119–7133.
47. Salm EJ, Dunn PJ, Shan L, Yamasaki M, Malewicz NM, Miyazaki T, Park J, Sumioka A, Hamer RRL, He WW, Morimoto-Tomita M, LaMotte RH, Tomita S. TMEM163 regulates ATP-gated P2X receptor and behavior. *Cell Rep* 2020; 31: 107704.
48. Lei X, Zeng J, Yan Y, Liu X. Blockage of HCN channels inhibits the function of P2X receptors in rat dorsal root ganglion neurons. *Neurochem Res* 2022; 47: 1083–1096.
49. Defaye M, Abdullah NS, Iftinca M, Hassan A, Agosti F, Zhang Z, Cumenal M, Zamponi GW, Altier C. Gut-innervating TRPV1+ neurons drive chronic visceral pain via microglial P2Y12 receptor. *Cell Mol Gastroenterol Hepatol* 2022; 13: 977–999.
50. Cherninskyi A, Storozhuk M, Maximyuk O, Kulyk V, Krishtal O. Triggering of major brain disorders by protons and ATP: the role of ASICs and P2X receptors. *Neurosci Bull* 2023; 39: 845–862.
51. Li YJ, Du WJ, Liu R, Zan GY, Ye BL, Li Q, Sheng ZH, Yuan YW, Song YJ, Liu JG, Liu ZQ. Paraventricular nucleus-central amygdala oxytocinergic projection modulates pain-related anxiety-like behaviors in mice. *CNS Neurosci Ther* 2023; 29: 3493–3506.
52. Antunes FTT, Huang S, Chen L, Zamponi GW. Effect of ABT-639 on Cav3.2 channel activity and its analgesic actions in mouse models of inflammatory and neuropathic pain. *Eur J Pharmacol* 2024; 967: 176416.
53. Guo H, Hu WC, Xian H, Shi YX, Liu YY, Ma SB, Pan KQ, Wu SX, Xu LY, Luo C, Xie RG. CCL2 potentiates inflammation pain and related anxiety-like behavior through NMDA signaling in anterior cingulate cortex. *Mol Neurobiol* 2024; 61: 4976–4991.
54. Dai X, Li L, Yan X, Fan Q, Wang R, Zhang W, Chen W, Liu Y, Meng J, Wang J. Myeloid Vamp3 deletion attenuates CFA-induced inflammation and pain in mice via ameliorating macrophage infiltration and inflammatory cytokine production. *Front Immunol* 2023; 14: 1239592.
55. Rahman MM, Hwang SM, Go EJ, Kim YH, Park CK. Irisin alleviates CFA-induced inflammatory pain by modulating macrophage polarization and spinal glial cell activation. *Biomed Pharmacother* 2024; 178: 117157.
56. Liu T, Stauber T. The volume-regulated anion channel LRRC8/VRAC is dispensable for cell proliferation and migration. *Int J Mol Sci* 2019; 20: 2663.
57. Wei M, Zhang G, Huang Z, Ding X, Sun Q, Zhang Y, Zhu R, Guan H, Ji M. ATP-$P2X_7$R-mediated microglia senescence aggravates retinal ganglion cell injury in chronic ocular hypertension. *J Neuroinflammation* 2023; 20: 180.
58. Zhang X, Wang M, Feng B, Zhang Q, Tong J, Wang M, Lu C, Peng S. Seizures in PPT1 knock-in mice are associated with inflammatory activation of microglia. *Int J Mol Sci* 2022; 23: 5586.
59. Peng Y, Li J, Luo D, Zhang S, Li S, Wang D, Wang X, Zhang Z, Wang X, Sun C, Gao X, Hui Y, He R. Muscle atrophy induced by overexpression of ALAS2 is related to muscle mitochondrial dysfunction. *Skelet Muscle* 2021; 11: 9.
60. Li YC, Tian YQ, Wu YY, Xu YC, Zhang PA, Sha J, Xu GY. Upregulation of spinal ASIC1 and NKCC1 expression contributes to chronic visceral pain in rats. *Front Mol Neurosci* 2020; 13: 611179.
61. Tang Y, Chen L, Liu B, Sun P, Chen Z, Huang Y, Ai-Qin C, Chen Y, Lin C. Spinal P2X4 receptors involved in visceral hypersensitivity of neonatal maternal separation rats. *Purinergic Signal* 2023; 19: 113–122.
62. Wu YY, Wang Q, Zhang PA, Zhu C, Xu GY. miR-1306-3p directly activates P2X3 receptors in primary sensory neurons to induce visceral pain in rats. *Pain* 2023; 164: 1555–1565.
63. Wu YY, Zhang HL, Lu X, Du H, Li YC, Zhang PA, Xu GY. Targeting GATA1 and p2x7r locus binding in spinal astrocytes suppresses chronic visceral pain by promoting DNA demethylation. *Neurosci Bull* 2022; 38: 359–372.
64. Wen L, Tang L, Zhang M, Wang C, Li S, Wen Y, Tu H, Tian H, Wei J, Liang P, Yang C, Li G, Gao Y. Gallic acid alleviates visceral pain and depression via inhibition of P2X7 receptor. *Int J Mol Sci* 2022; 23: 6159.
65. Athnaiel O, Cantillo S, Paredes S, Knezevic NN. The role of sex hormones in pain-related conditions. *Int J Mol Sci* 2023; 24: 1866.
66. Elina KC, Moon HC, Islam J, Kim HK, Park YS. The effect of optogenetic inhibition of the anterior cingulate cortex in neuropathic pain following sciatic nerve injury. *J Mol Neurosci* 2021; 71: 638–650.